Earth and Planetary Science Letters 345–348 (2012) 60–71

Contents lists available at SciVerse ScienceDirect

Earth and Planetary Science Letters

journal homepage: www.elsevier.com/locate/epsl

Letters

Microstructural and seismic properties of the upper mantle underneath a rifted continental terrane (Baja California): An example of sub-crustal mechanical asthenosphere?

L.N. Palasse [a,1], R.L.M. Vissers [a,*], H. Paulssen [a], A.R. Basu [b], M.R. Drury [a]

[a] Department of Earth Sciences, Utrecht University, P.O. Box 80.021, 3508 TA Utrecht, The Netherlands
[b] Department of Earth and Environmental Sciences, University of Rochester, Rochester, NY 14627, USA

ARTICLE INFO

Article history:
Received 29 August 2011
Received in revised form
22 May 2012
Accepted 18 June 2012
Editor: L. Stixrude

Keywords:
upper mantle xenoliths
Baja California
seismic anisotropy
lithosphere–asthenosphere boundary

ABSTRACT

The Gulf of California rift is a young and active plate boundary that links the San Andreas strike-slip fault system in California to the oceanic spreading system of the East Pacific Rise. The xenolith bearing lavas of the San Quintin volcanic area provide lower crust and upper mantle samples from beneath Baja California peninsula. The microstructures, crystallographic preferred orientations (CPO) and petrology of the San Quintin xenoliths suggest that the continental lithosphere in this region has undergone several stages of deformation, recrystallisation and melt–rock interaction. Melt–rock interactions have led to enrichment in olivine while fine-grained microstructures suggest intense deformation in an active shear zone in the shallow upper mantle. In this study we highlight the effect of the fine-grained mylonitic shear zone development in the upper mantle as an important process of weakening of continental lithosphere. The results of the microstructural study show a reduction in CPO strength with increasing grain size reduction. Most CPOs are consistent with dominant slip on the {0kl}[100] system. As a consequence, corresponding seismic anisotropies decrease for both P- and S-waves with increasing grain size reduction. The shallow crystallographic fabric can be related to active shear zones, which accommodate the relative motion between the Northern Baja terrane and the Pacific plate. Estimates of the strain rate, stress and viscosity indicate that the shallow mantle beneath Northern Baja is thermally and chemically lithospheric but mechanically has similar viscosity as the asthenosphere. The Northern Baja terrane is an interesting case of continental crust lying directly on low viscosity upper mantle.

1. Introduction

The Gulf of California is an active trans-tensional rift zone where the plate boundary evolves from continental extension in the north to an oceanic spreading system with transform faults in the south (Fig. 1). The upper mantle structure associated with this complex tectonic interaction between the Pacific, North American and now largely subducted Farallon plates has been recently studied using surface wave tomography (Zhang et al., 2007, 2009; Wang et al., 2009) inferred from the NARS-Baja seismic network (Trampert et al., 2003). The study of Zhang et al. (2009) using Rayleigh wave phase velocities suggests the presence of remnants of the Farallon microplate beneath the central and southern Gulf, whereas the existence of a low velocity zone in the northern part could be related to upwelling within a slab window. Zhang et al. (2009) found fast propagation directions of surface waves in the crust and uppermost mantle that are plate boundary parallel in the north and perpendicular in the south. Because olivine develops strong lattice preferred orientations during plastic deformation that may well account for this seismic anisotropy, there is a potential link between seismic anisotropy and upper mantle flow. Mantle xenoliths from the Holocene San Quintin volcanics in Baja California (Basu, 1975a, 1975b, 1977; Cabanes and Mercier, 1988; Storey et al., 1989; Luhr et al., 1995; Luhr and Aranda-Gomez, 1997) provide a unique opportunity to constrain the current petrophysics of this active area, and to test models for the regional variations in anisotropy.

The xenoliths exhibit a wide range of microstructures from deeper upper mantle coarse-porphyroclastic to shallow upper mantle fine-grained material. The objective of this study is to characterise the deformation history of the San Quintin xenoliths by performing a microstructural study, with measurements of the Crystallographic Preferred Orientation (CPO), to infer the anisotropic seismic properties of the mantle beneath the northern part of Baja California.

* Corresponding author. Tel.: +31 30 2535051.
E-mail address: rvissers@geo.uu.nl (R.L.M. Vissers).
[1] Present address: Bruker Nanoanalysis, Berlin.

0012-821X/$ - see front matter © 2012 Elsevier B.V. All rights reserved.
http://dx.doi.org/10.1016/j.epsl.2012.06.042

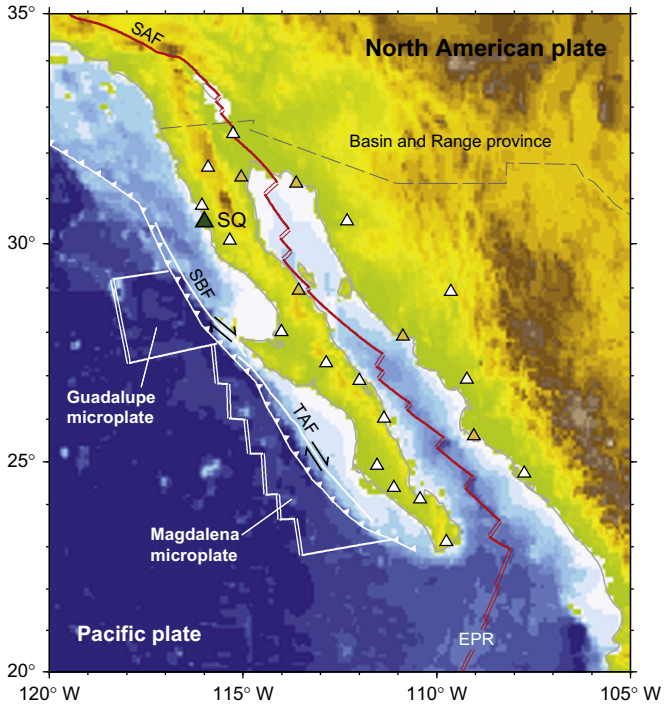

Fig. 1. Tectonic sketch map of the Gulf of California rift region, and location of the San Quintin volcanic field (indicated as "SQ") where upper mantle xenoliths have been brought up during Plio-Pleistocene volcanism. Present-day plate boundaries are shown. SAF: San Andreas Fault, EPR: East Pacific Rise, SBF: San Benito Fault, TAF: Tosco Abreojos Fault (modified after Zhang et al. (2007)). Triangles show locations of the NARS-Baja seismic network (Trampert et al., 2003).

In this paper we will use the terms asthenosphere and lithosphere in a mechanical sense, with "asthenosphere" to describe the low-viscosity upper mantle and "lithosphere" for the high-viscosity shallow upper mantle. In a tectonically active region, both lithosphere and asthenosphere may be actively deforming and the high-viscosity, mechanically defined lithosphere may not correspond to the seismically, chemically, or thermally defined boundary layers.

2. Tectonic setting of the San Quintin volcanics

The Gulf of California region is the result of tectonic interaction between the Pacific, Farallon and North American plates (Atwater and Stock, 1998; Plattner et al., 2007). The evolution of the oceanic tectonic plates is well known from the analysis of magnetic patterns on the ocean floor in combination with geological observations. The evolution after subduction is constrained by tomographic images of the present seismic velocity structure and modelling experiments (Zhang et al., 2009; Wang et al., 2009; Plattner et al., 2009).

Closely following the progressive south to north termination of subduction, the Pacific–Farallon spreading ridge reached the North American plate (28 Ma), and the plate boundary character changed from Farallon–North America oblique subduction to transcurrent motion with an extensional component taken up by North America (Stock and Hodges, 1989). Then, the Rivera triple junction migrated southward and the Farallon plate started to fragment into microplates. Subduction of the Guadalupe and Magdalena microplates beneath the region ceased at 12 Ma. The Pacific–North America plate motion was accommodated by strike-slip motion and extension in the future Gulf area, currently the Gulf Extensional Province. Over the last 10 Ma, the Gulf of California experienced a complex tectonic evolution subsequent to a complicated mountain building process along the western margin of the American plate and progressive interaction with the Pacific Ridge system. Present-day movements are thought to have been persistent over the last 5 Ma, with dextral transtension and movement of the Baja California Peninsula similar to the Pacific plate.

In zones of active deformation, direct information from the upper mantle can be obtained from upper mantle xenoliths. In the Gulf of California area upper mantle xenoliths were brought up during late Cenozoic volcanism in Baja California and Mexico (Fig. 1). In this study, we investigate 9 xenoliths of a previous study (Basu, 1977) from the San Quintin Volcanics along the Pacific coast of Baja California Norte. The Northern Baja crust is a continental terrane that rifted away from North America, and is currently also moving relative to the Pacific plate along faults like the San Benito (SBF) and Tosco Abreojos (TAF) faults (Plattner et al., 2007). The San Quintin volcanics consist of basaltic cinder cones with associated lava flows of late Pleistocene to recent age. This volcanic complex is the only one in the region where intraplate-type mafic alkalic magmas have erupted, carrying upper mantle and lower crustal xenoliths. We have selected seven peridotites with different microstructures and two pyroxenites. These latter are plagioclase-bearing pyroxenites, which likely represent the shallower mantle underneath the region and allow us to investigate possible relationships between different microstructures for different pressure and temperature conditions, to interpret these microstructures in terms of dominant deformation and recrystallisation mechanisms, and to estimate their seismic properties.

3. Microstructures of the xenoliths

About 80% of the ultramafic xenoliths from San Quintin are spinel lherzolites, with lesser harzburgites, dunites, and pyroxenites (Luhr et al., 1995). The suite is remarkable for the ubiquitous microstructural evidence of strong deformation (Basu, 1977; Luhr et al., 1995). Following Mercier and Nicolas (1975), the San Quintin xenoliths have been classified by Basu (1977) according to their increasing deformation, and include coarse granular, porphyroclastic, tabular mosaic and equigranular mosaic microstructures. The selection for the present study contains 9 samples, including 4 porphyroclastic, 3 tabular (with 2 pyroxenites) and 2 equigranular ones.

The porphyroclastic microstructure (samples SQ1-8-12, SQ2-69, SQ2-67 and SQ2-60) is the most abundant (Basu, 1977). It displays a bimodal grain size distribution, with large elongate porphyroclasts of olivine and pyroxenes (4–5 mm) and smaller spinel and clinopyroxenes in a finer matrix composed of neoblasts of the same mineral phases with grain sizes of up to $\sim$1.2 mm. The olivine porphyroclasts show undulatory extinction (Fig. 2) with well developed subboundaries. Many crystals have concave boundaries suggesting grain boundary migration, while the grain boundaries show triple junctions with near 120° angles. The neoblasts of the finer matrix are bimodally distributed with (1) a relatively large grain size of $\sim$1.2 mm similar to the subgrains within coarse olivines and (2) smaller grains of generally $\sim$0.6–0.3 mm and even smaller. Elongate olivine grains and aligned spinels define a foliation. Orthopyroxenes are not elongated but more rounded with irregular grain boundaries and kink bands, and seem to have a lattice preferred orientation, since exsolution lamellae (100) are often oriented parallel to the olivine elongation. Spinels have curvilinear boundaries without elongation. The neoblasts are free of deformation structures and exsolutions. In some samples (e.g. SQ2-60) the pyroxene porphyroclasts are rounded and occur within clusters.

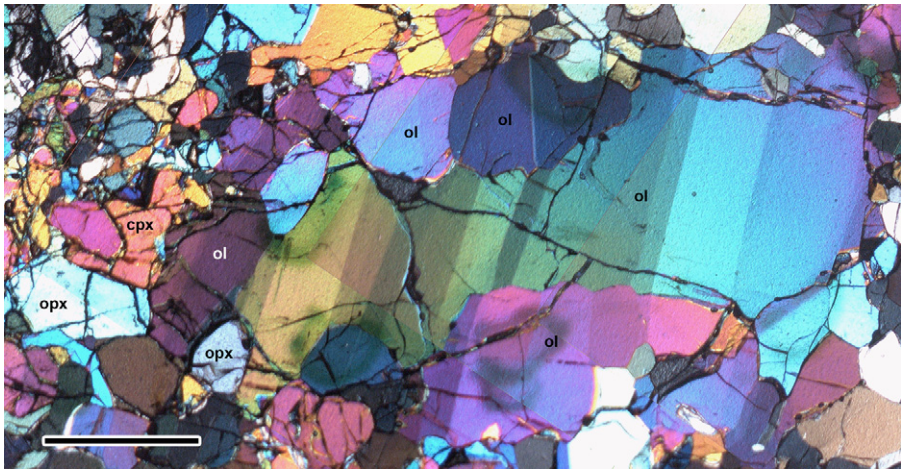

Fig. 2. Light micrograph (XPL) of typical porphyroclastic microstructure from the xenolith suite of San Quintin, with large olivine grains showing undulatory extinction with well-developed sub boundaries and 120° grain boundary triple junctions (sample SQ1-8-12). Note the presence, at the rims of the coarse grains, of small recrystallised grains (neoblasts) without sub-structures. Length of scale bar 1 mm, ol: olivine, opx: orthopyroxene, cpx: clinopyroxene.

The tabular mosaic microstructure (samples SQ2-17, SQ2-24 and SQ2-27) shows few relicts of porphyroclasts amidst a majority of tabular grains (Fig. 3a and b). In sample SQ2-27, few relict pyroxene porphyroclasts occur with very elongated shapes (Fig. 3c) parallel to the olivine elongation direction. Tabular olivines are between ~0.6 and 1.2 mm long, with straight grain boundaries at 120° triple junctions, and are oriented sub-parallel to the foliation (Fig. 3a). Note that samples SQ2-24 and SQ2-17 (with two thin sections a and b) are clinopyroxenites since the amount of clinopyroxene approaches 50% of the modal composition and the amount of olivine is below 5%. Moreover, sample SQ2-17 is plagioclase-bearing, with 38% of plagioclase in section SQ2-17a This sample has been selected since it contains plagioclase grains of similar sizes as the pyroxene tablet grains (Fig. 3d). Like the pyroxenes, plagioclase shows a bimodal grain size distribution, with grain diameters of ~1.4 and 0.4 mm.

Equigranular mosaic samples (SQ2-63, SQ2-68) are similar to the tabular ones but they rarely contain elongated pyroxene porphyroclasts (4 mm) within a fine-grained matrix (0.4 mm) of grains that are equant instead of tabular (Fig. 3e). Like in the above microstructures, the olivine grains display boundaries terminating at 120° triple junctions. The spinel alignment in the equigranular mosaic samples is stronger than that in the porphyroclastic and tabular mosaic ones.

The above grain-size reduction in the San Quintin xenoliths is accompanied by an increase in olivine content from 57% to 72%, a decrease in both types of pyroxenes from 20% in porphyroclastic to 10% in tabular and 8% in equigranular samples, and a decrease in spinel which is absent in some equigranular samples (Basu, 1977). Moreover, the porphyroclastic texture is the only one with clearly two generations of olivine and pyroxene, while both types of mosaic microstructures may contain two generations of pyroxenes (porphyroclast relicts and new grains) but only one generation of olivine grains.

Where the lineation is not clearly defined by the elongation of the grains and/or the alignment of spinels, Basu (1977) has described some additional structural evidence in the orthopyroxene deformation and recrystallisation like the development of retort shapes in opx, and exsolutions subparallel to the foliation. In the ultramafic xenoliths from San Quintin, orthopyroxene porphyroclasts are elongated and present undulatory extinction and kink bands. Recovery structures in the pyroxenes such as polygonization and subgrain formation are rare compared with the olivines. Nucleation of new orthopyroxene takes place along kink band boundaries and is associated with clinopyroxene exsolutions as well. In tabular and equigranular specimens, enstatite grains are often aggregated and aligned within the direction of spinel alignment, and they are occasionally elongated in this direction.

4. Crystallographic fabrics (CPO)

Crystallographic orientations were measured using Electron Back Scattered Diffraction (EBSD) on a Scanning Electron Microscope (SEM) (Fig. 4). We note that three samples (SQ1-8-12, SQ2-60 and SQ2-17a, b) do not show a very clear foliation or lineation. The CPOs were manually indexed to prevent errors due to the pseudo-hexagonal symmetry of olivine in the [100] direction. One point per grain was measured for at least 150 olivine grains and 50 pyroxene grains, which is usually sufficient to calculate representative CPO strengths (Ben Ismaïl and Mainprice, 1998).

4.1. CPO measurements

The results are shown in Fig. 4a, b and c for the olivine, orthopyroxene and clinopyroxene respectively, with the CPOs represented with respect to the spinel foliation and lineation where identified, to allow convenient interpretation in terms of slip systems. In addition, Fig. 4c shows a plagioclase CPO from pyroxenite sample SQ2-17.

Irrespective of their modal composition, porphyroclastic lherzolites (SQ1-8-12, SQ2-69, SQ2-67 and SQ2-60) show strong and well developed olivine CPOs that are characterised by a concentration of [100] axes close to the lineation defined by spinel and/or olivine elongation, and with [010] mainly perpendicular to the foliation with a tendency to form a girdle perpendicular to the lineation (Fig. 4a). These olivine CPOs suggest a deformation by dislocation creep, with activation of the {0kl}[100] or (010)[100] slip systems. The observed CPOs are the common upper mantle fabrics for low water content being D-type and A-type (Jung and Karato, 2001).

The tabular peridotite SQ2-27 has a slightly different olivine CPO, with [100] strongly concentrated along the lineation, and both [010] and [001] almost perpendicular to this direction. The olivine CPO is intermediate between an A-type (Jung and Karato, 2001) and an E-type CPO, which occurs at higher water content than the A-type and D-type (Mehl et al., 2003; Katayama et al.,

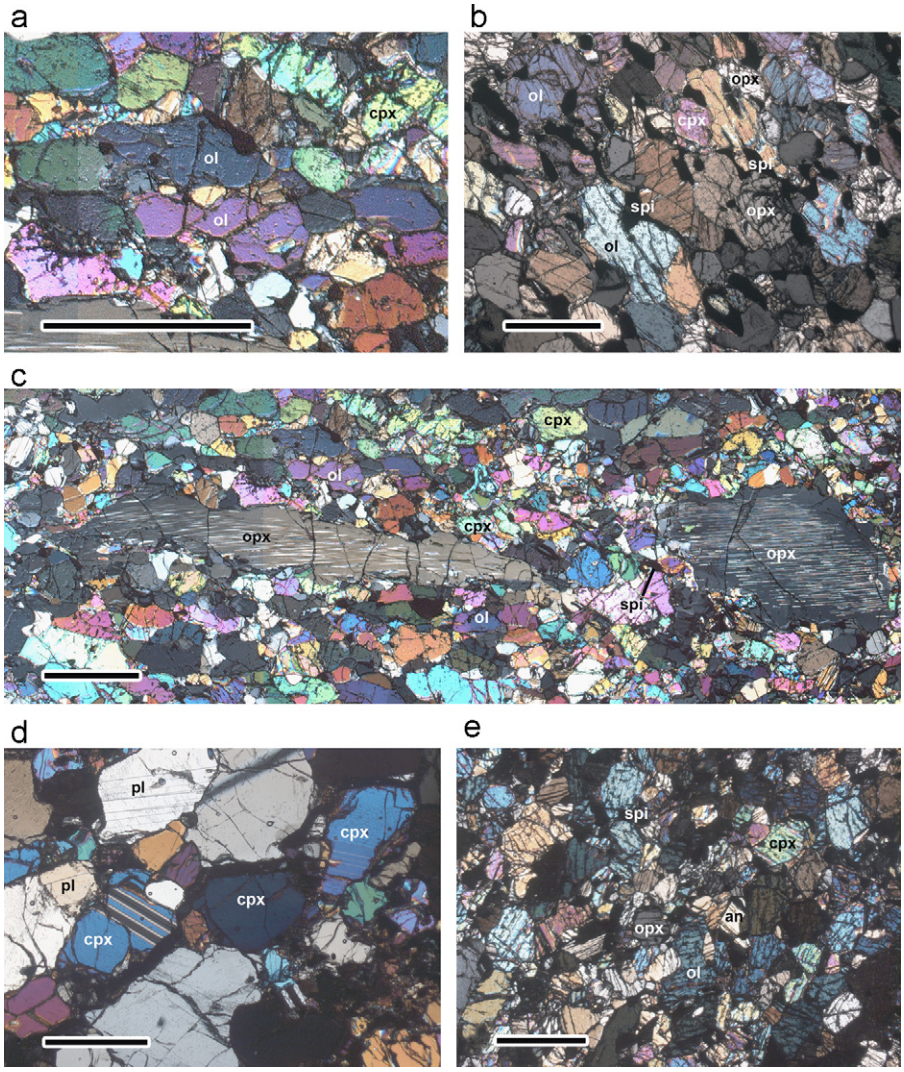

Fig. 3. Light micrograph (XPL) showing different mosaic microstructures from the xenolith suite of San Quintin. Length of scale bar 1 mm in all diagrams, ol: olivine, opx: orthopyroxene, cpx: clinopyroxene, spi: spinel, pl: plagioclase, an: anorthite. (a) Tabular mosaic microstructure of sample SQ2-27. Note 120° grain boundary triple junctions. (b) Tabular mosaic microstructure of pyroxenite sample SQ2-24 containing a few relicts of porphyroclasts amidst a majority of tabular grains. (c) Orthopyroxene porphyroclast remnants in tabular peridotite sample SQ2-27, with strongly elongated shapes aligned parallel to the olivine elongation direction in the mosaic matrix. (d) Tabular mosaic microstructure of plagioclase-bearing pyroxenite SQ2-17. (e) Equigranular mosaic microstructure of sample SQ2-63 with similar grain size as the tabular microstructure but dominated by equant grains. Note that there are almost no porphyroclasts.

2004). The pyroxenes present a somewhat scattered CPO. The equigranular peridotites (SQ2-63, SQ2-68) display the same CPO as the porphyroclastic xenoliths (Fig. 4a).

In all of the above samples, the pyroxene CPOs are not strong and they are not the pyroxene CPOs commonly associated with those of the olivine {0kl}[100] slip in upper mantle peridotites. It is usually observed that with the {0kl}[100] olivine slip system, the pyroxenes have their [001] axis along the lineation (Nicolas, 1986). In the above xenolith samples, however, the [100] axes of the clinopyroxenes are mainly aligned with the lineation (instead of [001]). In the porphyroclastic samples SQ1-8-12 and SQ2-69, the tabular sample SQ2-27 and in the equigranular sample SQ2-63, the clinopyroxene [100] axes are aligned with olivine [100], suggesting (001)[100] slip in clinopyroxene characteristic of low temperature conditions. In the porphyroclastic sample SQ2-67 the orthopyroxene CPOs seem to be coherent with the usual mantle olivine CPO since the orthopyroxene [001] axes concentrate along the lineation and [100] and [010] are perpendicular suggesting activation of the (100) [001] system. In most samples the orthopyroxene CPO is weak and scattered and is difficult to interpret in terms of active slip systems.

The tabular pyroxenite SQ2-17 contains a large amount of plagioclase. In this specimen, the plagioclase grains are well oriented, in particular the large grains which display a strong orientation of the [001] axis oblique to the lineation, while the smaller grains display some randomisation of their CPOs. The pyroxene CPOs from SQ2-17a, however, are scattered with only few large orthopyroxenes oriented like the plagioclase grains. The plagioclase CPO (Fig. 4c) suggests activity of the (010) [001] slip system (Nicolas and Poirier, 1976).

In all of the peridotites samples, we have compared the coarse grain (or remnants of coarse grain) CPOs with the neoblast orientations. It appears that, for all minerals, the neoblast CPOs are similar to the CPOs from the coarse-grained fractions, but with a more scattered distribution.

4.2. *Inferring the slip system by EBSD mapping*

Although the foliation and lineation are not always clearly displayed by the grain shapes, most porphyroclastic and mosaic peridotites have a similar type of CPO consistent with {0kl}[100] slip. In the porphyroclastic samples the main [001] maximum is at

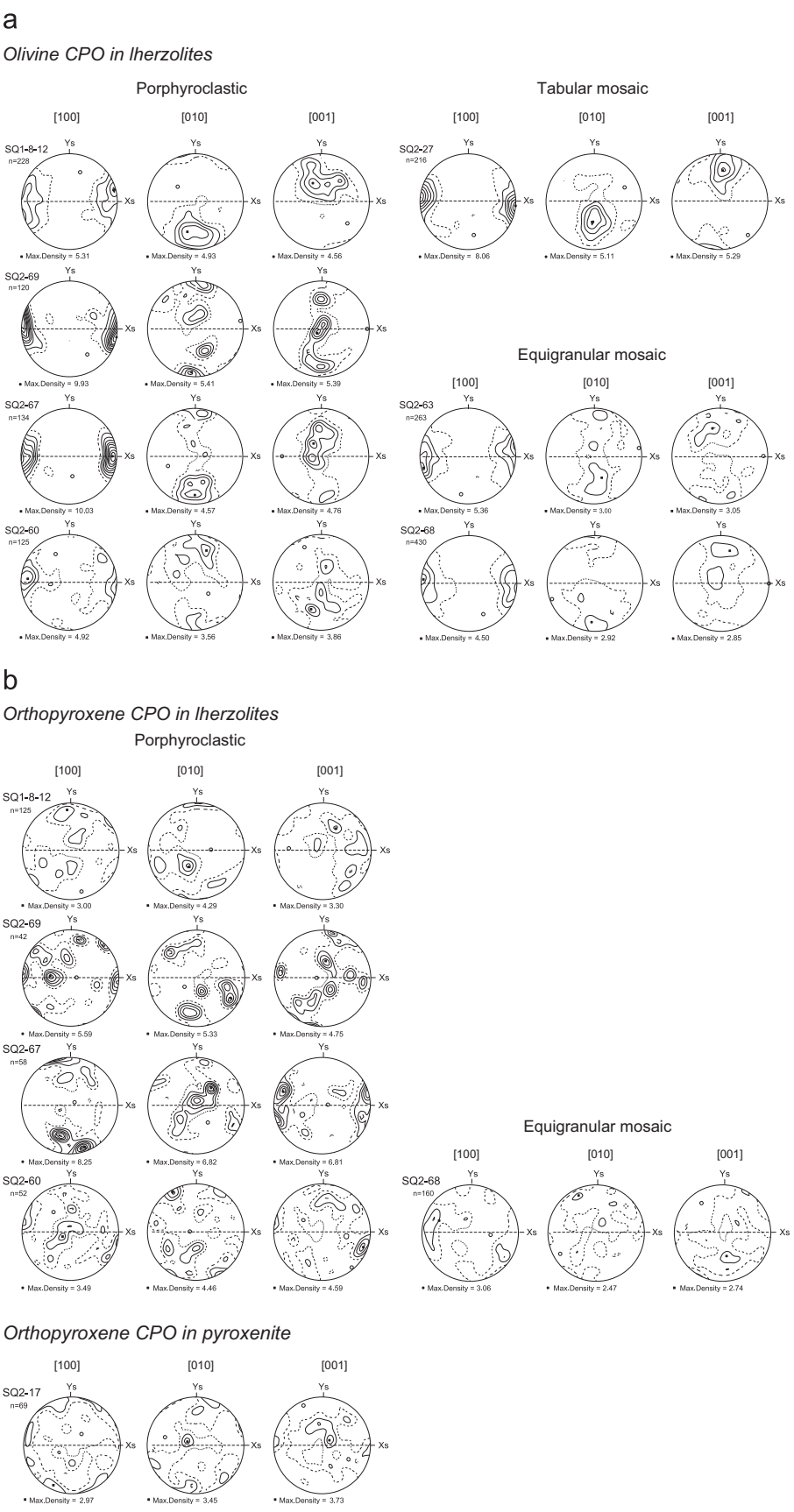

Fig. 4. Crystallographic preferred orientations (CPOs) of the different mineral phases from the San Quintin xenoliths, assessed using electron back-scattered diffraction (EBSD). The foliation inferred from the elongation of the grains and/or the spinel alignment is shown as EW, with the lineation in the foliation plane horizontal. All diagrams are equal-area, lower hemisphere projections, *n* measurements, contoured at multiple times uniform distribution except for pyroxene CPOs with ≤ 50 measurements. (a) Olivine CPOs, (b) relevant orthopyroxene CPO's, (c) representative clinopyroxene CPOs, and one anorthite CPO (sample SQ2-17).

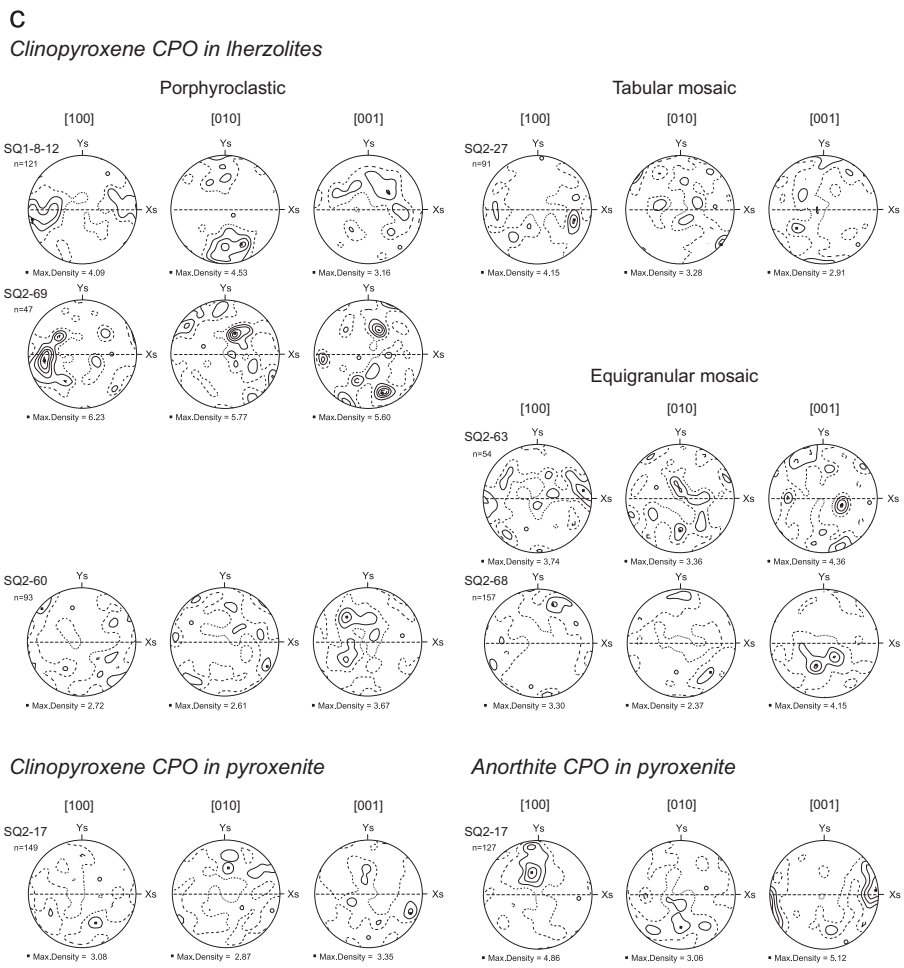

Fig. 4. (*continued*)

low angle to the foliation, while in the mosaic samples the main [001] maximum has a high angle to foliation. This suggests the possibility that slip on the (010) plane was more important in the porphyroclastic samples and slip on the (001) plane more important in the mosaic samples, although the difference is not very strong.

The active olivine slip system can also be identified using the subgrain boundaries and rotation axes (Lloyd et al., 1991). In order to test whether or not intracrystalline deformation in porphyroclastic and mosaic peridotites was accommodated by different slip systems, the olivine subgrain boundaries have been investigated by EBSD mapping on large olivines in samples SQ1-8-12, SQ2-27 and SQ2-60, to constrain the different olivine active slip systems. In the porphyroclastic sample SQ1-8-12, the EBSD map (Fig. 5a) shows (100) boundaries, which indicate a [100] slip direction. In addition, the slip system can also be inferred from inverse pole figures for misorientation axes. The results reveal a range of misorientation axes characteristic of (010)[100], {0kl}[100] and (001)[100] slip systems (Fig. 5b). For the tabular SQ2-27 sample, the EBSD map indicates that olivine subgrain boundaries have their rotation axis mostly along [001], suggesting (010)[100] slip. The combined information from the CPOs and subgrain misorientation axes suggests that similar olivine slip systems were activated in all xenolith types.

5. Seismic properties of the San Quintin, Baja California lithosphere

To constrain the effect of the compositional and microstructural changes induced by deformation on the upper mantle seismic properties at different depths, we have estimated the three-dimensional distributions of seismic velocities. With this aim, the individual grain elastic constant tensors are averaged for each sample as a function of the crystallographic orientations and modal composition at ambient upper mantle conditions, and we calculated Voigt–Reuss–Hill averages, using software developed by Mainprice (1990) and available via the internet (〈http://www.gm.univ-montp2.fr/PERSO/mainprice/〉). The CPO measurements were made with one point per grain, which means that the volume fraction of porphyroclasts will be underrepresented, and the seismic anisotropy estimates are biased to the smaller recrystallised grains in the porphyroclastic samples.

Lherzolites with porphyroclastic and equigranular microstructures display compressional (*P*) wave velocity distributions and shear (*S*) wave anisotropy patterns (Fig. 6) typical of upper mantle rocks deformed under high temperature. The anisotropy is characterised by the fastest propagation of the P-wave parallel to the lineation, that is parallel to the maximum concentration of olivine [100] axes, and the slowest when propagating normal to the foliation, that is parallel to the maximum concentration of the [010] axes. Samples SQ2-67, SQ2-69 and SQ1-8-12 are highly anisotropic. The P-wave azimuthal anisotropy varies from 8.3% to 10.2% and the S-wave polarisation anisotropy varies from 5.0% to 6.9%. The polarisation anisotropy is minimal for S-waves propagating at low angles to the lineation and maximum for those propagating at high angles to the lineation. The highest anisotropies are displayed by the porphyroclastic samples in which the olivines show a strong CPO.

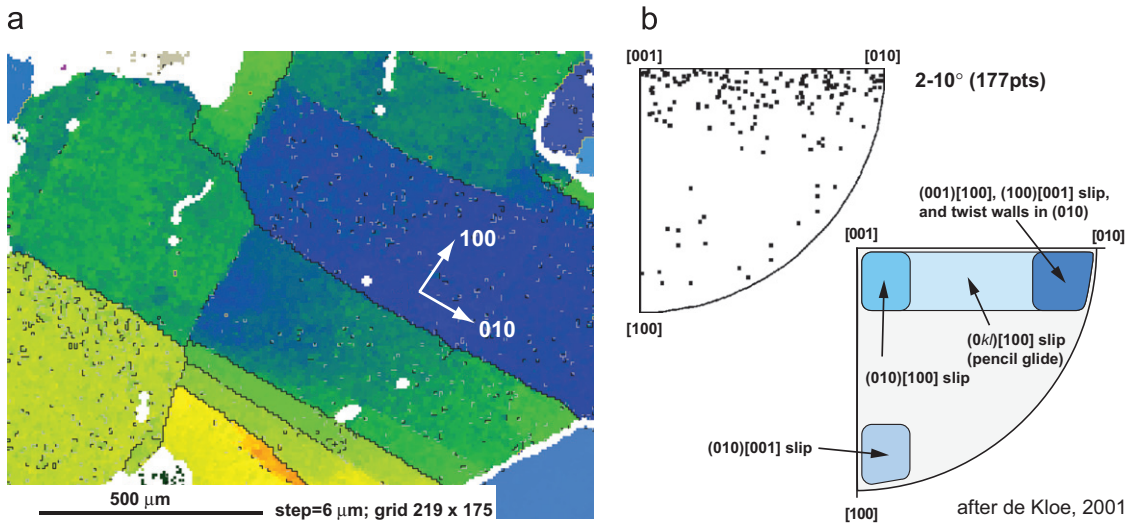

Fig. 5. (a) EBSD orientation map of porphyroclastic olivine in sample SQ1-8-12. The map shows well developed (100) boundaries indicating a [100] slip direction. Grey tones reflect the orientation of the olivine (defined by the Euler angles), domains in white are non-indexed measurements. The corresponding olivine CPO is shown in Fig. 4a. (b) The olivine slip system is inferred from the distribution of misorientation axes in the inverse pole figure, which are compared with the misorientation axes distribution expected for different slip systems in olivine by De Kloe (2001). See text for further explanation.

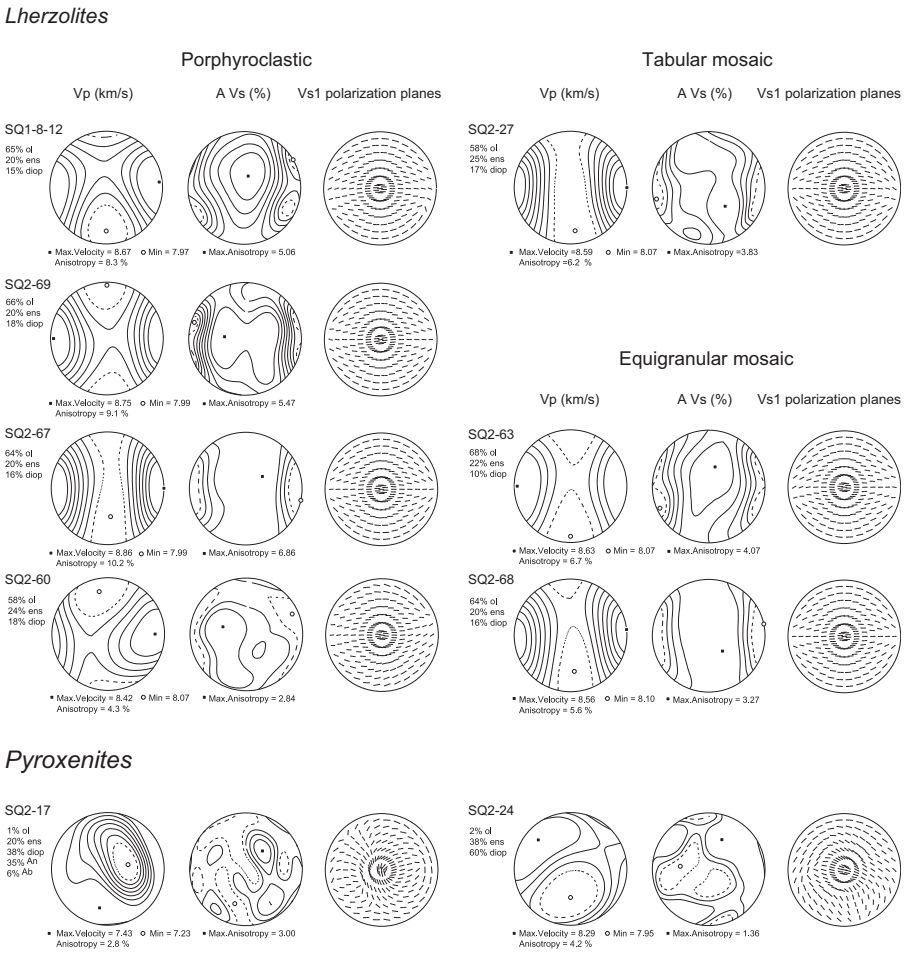

Fig. 6. Modelled three-dimensional compressional wave velocity and shear wave anisotropy (intensity and polarisation direction of the fast wave) distributions for the samples presented in Fig. 4. All diagrams are equal-area, lower hemisphere projections, contoured for P-waves velocities and S-wave anisotropy at 0.1 km/s and 1% intervals, respectively. Diagrams are shown in the same orientations as in Fig. 4, with the foliation EW and the lineation horizontal.

The porphyroclastic sample SQ2-60, the tabular SQ2-27 and the equigranular SQ2-63/68 are less anisotropic, with P-wave azimuthal anisotropy values around 4.0–6.7% and an S-wave polarisation anisotropy between 2.8% and 4.0%. Since the porphyroclastic samples display the highest P- and S-wave anisotropies while the lowest are displayed by the mosaic lherzolites,

there seems to be a relationship between microstructure and seismic properties. Although they are weaker, the P- and S-wave velocity and anisotropy distribution patterns of the finer grained lherzolites are similar to those of the porphyroclastic samples. Note that the weakest anisotropies are displayed by the pyroxenites SQ2-17 and SQ2-24. Compared with all the lherzolites, the pyroxenite SQ2-24 has the fastest P-wave propagation direction between the maximum concentration of the [100] axes of the olivine (only 5% in the sample) and pyroxenes and the slowest propagation is strongly influenced by the distribution of the [010] and [001] of both pyroxenes. The presence of plagioclase rich pyroxenites with weak CPOs is likely to reduce the anisotropy of the shallow upper mantle beneath San Quintin.

In addition, we have calculated the delay times according to the seismic properties of the studied samples with

$$\delta t = \mathrm{LAVs}/100\mathrm{Vs}$$

for different S-wave propagation and different layer thickness (L in km) and sample orientation as displayed in Fig. 4, where AVs (in %) and Vs (in km/s) are the shear wave velocity anisotropy and average shear wave velocity, respectively. A layer of at least 115 km thick composed of porphyroclastic peridotite (such as sample SQ2-69 with 5.5% shear wave velocity anisotropy) would, for a vertical incidence of the waves, explain the SKS delay times of 1.2–1.3 s in the San Quintin area (see the results of Obrebski et al. (2006), and Long (2010) for nearby seismic station NE72). In contrast, for a vertical incidence and a layer thickness of 120 km, mosaic microstructures would contribute to 60% of the observed anisotropy, while the pyroxenite samples for those same conditions would contribute to only 30%. As the seismologically defined lithosphere beneath San Quintin is likely to be much less than 100 km, it is clearly not thick enough to account for the magnitude of the reported SKS splitting. It is not possible to compare the SKS direction of fast polarisation with the samples because the orientations of the samples are unknown.

6. Implication for the observed seismic properties of the Northern Baja mantle

The microstructures of the studied xenoliths, which sample the upper mantle beneath a rifted continental terrane, are characteristic of ductile deformation and recrystallisation in the pertinent upper mantle. During this process, strong CPOs are developed, leading to distinct seismic velocity anisotropies. We now compare the calculated seismic properties from the xenoliths' CPOs with the observed seismic anisotropic properties obtained by the NARS-Baja seismic network data.

6.1. Deformation history of the San Quintin mantle xenoliths

Prior to their entrainment in the basalt (Basu, 1975b), the studied xenoliths were affected by plastic deformation, recrystallisation and melt–rock reactions at upper mantle conditions. The observed reduction in anisotropy in the strongly recrystallised lherzolites and pyroxenitic samples can thus be interpreted partly as the result of dispersion of the olivine CPO due to (1) the recrystallisation of olivine neoblasts with a wider range of orientations than porphyroclasts, and (2) an increased role of grain boundary sliding in the fine grained olivine matrix. In addition to recrystallisation processes, the decrease in anisotropy might also be related to melt/rock reactions that have affected the rocks, with the enrichment in olivine by magma injection and/or partial melting giving crystallisation of new and sometimes randomly oriented grains, e.g. Tommasi et al. (2004). These processes may have changed the modal composition and the microstructures and hence, the seismic velocity properties. The clinopyroxenites have been interpreted to result from magma injection into the host-peridotite prior to the main deformation (Basu, 1975b), since these rocks show the same deformation microstructures as the host peridotites. On the other hand, they injected after the major melting event as the peridotites are severely depleted in lithophile elements (Basu and Murthy, 1977; Cabanes and Mercier, 1988).

The spatial distribution and structural relationships between different mantle lithologies of the San Quintin xenoliths may be inferred to result either from different extraction depths, to explain the amount of plagioclase in some rocks, or from melt–rock interactions that take place, for example, in response to km-scale melting and percolation fronts associated with thermal erosion of lithospheric mantle (Lenoir et al., 2001). In a study of the isotopic compositions of the San Quintin samples, Luhr et al. (1995) have demonstrated that the most differentiated, xenolith carrying magmas can be modelled by fractional crystallisation of olivine, plagioclase, clinopyroxenes and spinel from primitive magmas. Primitive magmas present in even the youngest cones of San Quintin (with high Mg# content) show rising Al_2O_3 and decreasing CaO with decreasing incompatible element abundances, suggesting progressive partial melting of spinel lherzolite at unusual shallow upper mantle levels, followed by contamination of the magmas with low $^{206}Pb/^{204}Pb$ and high $^{87}Sr/^{86}Sr$-bearing crustal components. The presence of occasional quartz xenocrysts in these lavas further attests this scenario.

According to Cabanes and Mercier (1988), the recorded equilibrium temperatures obtained with different exchange geothermometers are consistent and show two distinct records: (1) temperatures of 1000–1050 °C and pressures $P < 2$ GPa recorded by the coarse grained rocks during their last equilibrium, and (2) lower temperature of 800–950 °C and a lower minimum equilibrium pressure $P < 1$ GPa for the last equilibrium of the porphyroclastic and mosaic (tabular and equigranular) peridotites. Similar results were obtained by Luhr and Aranda-Gómez (1997) who found that the transition from porphyroclastic to mosaic microstructures is accompanied by a decrease in calculated equilibrium temperatures from 1105 °C to 910 °C (Luhr and Aranda-Gómez, 1997), a decrease in pressure estimated from the Ca in olivine and a change in major element composition. This suggests that the host basalts have sampled peridotites from different mantle levels.

To explain the simultaneous sampling of these different peridotites and pyroxenites, Basu (1975a) has suggested that plastic deformation occurred during diapiric ascent of mantle material from the asthenosphere, with the host magmas originating from partial melting at the base of this diapir. Our study of the different microstructures has revealed CPOs for most of the different mineral phases, except for the random CPOs displayed by secondary, principally pyroxene grains. If plastic deformation would have occurred during diapiric ascent, only the primitive microstructure would have developed CPOs, whilst the random orientation of the fine secondary grains could be related to recent partial melting and melt rock reaction. In any case, since the different microstructures yield different equilibrium conditions and different CPOs for a relatively small extraction area ($\sim 10\ \mathrm{km}^2$), and because of the increase in plagioclase content with increasing deformation, it seems likely that the xenoliths represent different upper mantle levels.

In contrast to Basu's hypothesis, Cabanes and Mercier (1988) have suggested that the ascending magma promoted hydraulic fracturing in the coarse-grained lherzolites, while at shallower depth it sampled an active shear zone containing the highly deformed porphyroclastic and mosaic microstructures and plagioclase rich rocks. A shallow active shear zone would explain the formation of

low P–T deformed xenoliths above a less deformed deeper mantle, yielding different compositions and equilibrium conditions.

Although plastic deformation can certainly contribute to the development of porphyroclastic microstructures, we suggest that dynamic recrystallisation is not the principal process responsible for the formation of neoblasts since they are much smaller than the subgrains within the porphyroclasts and because most of them display weak CPOs. In addition, the progressive dispersion of the olivine CPOs is associated with smaller grain sizes. In the porphyroclastic texture, the neoblasts are bimodally distributed (Fig. 2a) with the largest neoblasts likely originating from dynamic recrystallisation of coarse grains, as opposed to the smaller interstitial neoblasts, which may have formed by melt–rock interaction. Late crystallisation during melt–rock reaction, prior to the last deformation (Basu, 1977; Cabanes and Mercier, 1988), would explain the presence of numerous small and variably oriented neoblasts in the porphyroclastic specimen, like the small orthopyroxenes in SQ2-60 and SQ1-8-12. In the mosaic mantle rocks, the grain size is uniform by definition except for few relicts of pyroxene porphyroclasts but the pyroxenes' CPOs can be random too (SQ2-68). In the case of melt–rock interaction, the weak CPOs could be the result of the opposing effects of intense melt–rock reaction on one hand and higher strains on the other, possibly generated within a shallow active shear zone. The weakening effect of melt–rock interaction on olivine CPOs has been demonstrated in the French Polynesia xenoliths (Tommasi et al., 2004) and in the Massif Central xenoliths (Palasse, 2003). Moreover, melt–rock interaction would explain the dissolution of pyroxene and crystallisation of olivine in porphyroclastic and mosaic textures as suggested by the increase in olivine at the expense of the pyroxene content (Holtzman and Kendall, 2010).

Most of the porphyroclastic xenoliths studied show a strong olivine CPO characteristic of slip mainly on the {0kl}[100] family of slip systems. Increasing deformation led to the development of tabular and equigranular microstructures in the shallower mantle, with a possible increased role for slip on (001)[100] which has been identified in the Baja California xenoliths samples by Zeuch and Green (1977). A transition in slip system from {0kl}[100] to (001)[100] has been described by Katayama et al. (2004) with increasing water content (see also Karato (1995)). The water contents in the San Quintin xenoliths have been measured by Peslier et al. (2002) and Peslier and Luhr (2006) using the Bell et al. (2003) calibration, demonstrating that the xenoliths contain some water, with 77–154 ppm H_2O by weight for the whole rock, 0–6.6 ppm H_2O by weight in olivine with 40% hydrogen loss, and 38–477 ppm H_2O by weight in pyroxenes. Using the Bell et al. (2003) calibration and taking the hydrogen loss into account, the maximum of water content in olivine will be 11 ppm by weight, which corresponds to 3.14–4.4 ppm by weight according to Paterson's (1982) calibration. Thus, even if the pyroxenes are much more water-rich than the olivine grains, these olivine water contents are too low to fit in the range reported by Katayama et al. (2004) for the E-type CPO ranging from 16 to 40 ppm H_2O by weight according to Paterson's (1982) calibration. Thus in the case of the Baja xenoliths the E-like CPO in the tabular mosaic sample SQ2-27 has developed in relatively dry olivine. While there is some evidence for changes in the relative activity of the slip systems between the porphyroclastic and mosaic samples, the CPOs in both xenolith types are consistent with {0kl}[100] slip in dry olivine, which implies deformation temperatures less than about 1000 °C (Carter and Avé Lallemant, 1970).

6.2. Implications for the seismic structure of the Gulf of California

The seismic properties of the studied San Quintin xenolith suite, calculated from the CPO data, suggest that in all xenolith types the fast P-wave direction is aligned along the direction of upper mantle flow. The orientation of the olivine [001] and [010] axes has minor effect on the seismic velocities (see Fig. 6). In this situation, the fast propagation direction (i.e. the azimuthal anisotropy) and the polarisation of the faster S wave are sub-parallel to the shear direction. The increase in plastic deformation demonstrated by the increased deformation of orthopyroxene porphyroclasts (Basu, 1977) would be expected to increase the seismic anisotropy, however, melt–rock interaction would be responsible for the growth of variably oriented grains which scatter the pertinent CPOs and consequently decrease seismic anisotropies. Furthermore, the grain size reduction produced by recrystallisation and melt rock reaction may increase the role of grain boundary sliding, which can also account for the weakening of the CPO. The seismic properties are also considerably affected by the increase in pyroxene content such as the presence of clinopyroxenite veins. In the San Quintin xenoliths, most of the clinopyroxenes have a weak CPO except in the coarse porphyroclastic sample SQ1-8-12 where the distribution of the pyroxene axes is parallel to the olivine ones. In this case, the distribution of clinopyroxene axes enhances the seismic anisotropy but this effect is counterbalanced by the random orientation of the secondary orthopyroxenes in this sample. Most of the orthopyroxenes in the different microstructures have a weak CPO and thus tend to decrease seismic anisotropies. However, the orthopyroxenes in the porphyroclastic samples SQ2-67 and the coarse ones in SQ2-60 and SQ1-8-12 exhibit the usual upper mantle CPO, with [001] along, and [100] perpendicular to the lineation. But this orientation will lower the anisotropies since the fast P-wave distribution in orthopyroxene differs from the olivine because [100] is aligned to the lineation.

We will now compare the seismic properties inferred from our peridotite samples with seismological data of the region obtained using the NARS-Baja seismic network (Zhang et al., 2007, 2009). There are uncertainties in relating these seismological data to the anisotropy calculated for the xenoliths because the foliation and lineation orientations at depth are unknown. Using the NARS-Baja network, Zhang et al. (2007) have determined the anisotropic Rayleigh wave phase velocity. Fig. 7 shows the fast propagation directions for three periods which have different depth sensitivity in the crust and uppermost mantle. A figure of the depth sensitivity kernels at these three periods is presented in the supplementary material. The azimuthal anisotropy results show that the fast directions of phase velocities with crustal and shallow mantle sensitivity (period $T=14$ s) change from predominantly plate-boundary parallel in the north to plate-boundary perpendicular in the south. The transition occurs where the plate boundary changes from a region of diffuse transtensional continental deformation to a system of oceanic-type spreading (Nagy and Stock, 2000). Zhang et al. (2007, 2009) have interpreted the low velocity anomaly and small values of azimuthal anisotropy beneath the plate boundary on the 30 s phase velocity map (with predominant mantle sensitivity to depths less than $\sim$90 km) as being due to ridge-associated upwelling beneath the Gulf, while high velocity anomalies indicate the presence of the Guadalupe and Magdalena slab remnants attached to the southern part of the Baja California peninsula.

Storey et al. (1989) have demonstrated that the San Quintin lavas are derived from an asthenospheric source and might be related to cessation of plate subduction beneath the peninsula and that the source region may overly a slab window. Beneath San Quintin, the crust has a typical thickness of 30–35 km (Lewis et al., 2001; Persaud et al., 2007) and the fast-propagation direction at crustal and shallow mantle depths is parallel to the plate boundary (Fig. 7, Zhang et al., 2007). In the southern part of the peninsula, the fast propagation is perpendicular to the

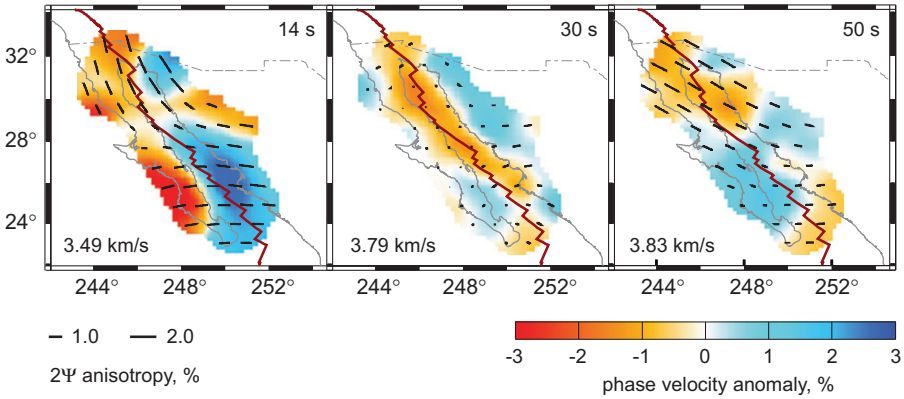

Fig. 7. Tomographic images of Rayleigh wave phase velocity after Zhang et al. (2007) for relevant periods. The period shown in the upper right corner is characteristic of the depth: 14 s is for crustal and uppermost mantle sensitivity, 30 s for lower crust-upper mantle sensitivity (<90 km, maximum sensitivity at $\sim$45 km) and 50 s for mantle sensitivity (<150 km, maximum sensitivity at $\sim$75 km). The colour bar indicates the phase velocity anomaly relative to the average phase velocity at that period given in lower left corner. The black bars indicate the size of the anisotropy. The thick red line indicates the plate boundary. (For interpretation of the references to colour in this figure legend, the reader is referred to the web version of this article.)

opening where a relict of the subducting slab would be preserved. Northern Baja has also been affected by past subduction. The olivine slip systems found in the San Quintin xenoliths are not consistent with subduction zone CPOs where [001] slip may occur (Jung and Karato, 2001; Kneller et al., 2005), but we note that such predictions may not be valid in all cases (Mehl et al., 2003; Soustelle et al., 2010).

7. Discussion

The CPOs documented in the San Quitin xenoliths might be related to the current mantle flow or could be frozen CPOs from an earlier stage. As argued above, the plagioclase-rich xenolith samples and the finer grained mosaic xenoliths from the San Quintin volcanics represent shallow upper mantle. According to the tomographic images for periods of 14 s, the flow direction at lower crustal and uppermost mantle depths is along the plate boundary. The anisotropy is rather homogeneous, with a NNW–SSE direction throughout the Northern Baja peninsula. From the xenolith CPOs we can infer that the anisotropy can be related to a NNW–SSE orientation of the [*a*] axis maxima. Such an orientation could be produced by lithosphere-scale homogeneous transcurrent shear in the shallow mantle (e.g., Vauchez and Tommasi, 2003). Alternatively, the homogenous anisotropy in the shallow mantle could be related to sub-horizontal shear in the shallow mantle which decouples the deeper mantle from the Baja lower crust. In both cases the current deformation may be associated with the relative motion between northern Baja and the Pacific plate (Plattner et al., 2007, 2009). This motion of 4–6 mm/yr is accommodated in the upper crust by faults offshore Baja and one of these faults occurs close to the San Quintin volcanics (Plattner et al., 2007).

The coarse porphyroclastic samples from the deeper spinel stability field are probably derived from depths corresponding to the Rayleigh images for periods of 30 s, which are sensitive to depths from 15 to 150 km, with a maximum sensitivity around 40–50 km. However the azimuthal anisotropy in the 30 s map is small. As the granular and porphyroclastic xenoliths have high anisotropy, the lack of azimuthal anisotropy on the 30 s phase velocity map might reflect vertical upwelling or an isotropic structure on the scale sampled by the seismic waves. On the 50 s map, the anisotropy is the highest and the inferred mantle flow is oriented ENE–WSW. The 50 s data have a maximum sensitivity to depths of 70–100 km, corresponding to the deeper part of the spinel lherzolite and the garnet lherzolite PT field, and most of the San Quintin xenoliths are derived from shallower depths.

Our results on xenolith CPO and anisotropy show that the rock-scale anisotropy increases with depth since the shallower samples with mosaic microstructures and/or those from the plagioclase stability field present the lowest anisotropy, while the deeper porphyroclastic xenoliths are the most anisotropic. One tabular mosaic xenolith has an E-like CPO. Karato et al. (2008) suggest that E-type CPOs reflects low stress and moderate to high water content. However, the San Quintin xenoliths contain very little water.

The flow stress and viscosity of the shallow mantle shear zone beneath San Quintin can be estimated from the microstructures, water content and olivine flow laws. Temperatures of about 900 °C are appropriate for the porphyroclastic and mosaic xenoliths (Luhr and Aranda-Gomez, 1997). The strain rate can be estimated by assuming that the motion between the northern Baja Peninsula and the Pacific plate of between 3 and 6 mm/yr is accommodated in shear zones, giving equivalent uniaxial strain rates of $1.1–5.7\times10^{-14}\,s^{-1}$ for a 1 km thick zone and $1.1–5.7\times10^{-15}\,s^{-1}$ for a 10 km thick zone. A flow stress of around 10–30 MPa can be estimated from the olivine neoblast grain size in the mosaic xenoliths using the Van der Wal et al. (1993) olivine piezometer, while dry olivine flow laws (Hirth and Kohlstedt, 2003) suggest a flow stress of 10–40 MPa. Combining the strain rate and stress estimates we obtain estimates for the shear zone viscosity in the range of $4.4\times10^{19}–3.5\times10^{20}$ Pa s for a 1 km thick shear zone and $4.4\times10^{20}–3.5\times10^{21}$ Pa s. for a 10 km thick shear zone. The finer grained equigranular rocks are predicted to have lower viscosity than the coaser grained tabular and porphyroclastic xenoliths within the range reported above. These estimates of shallow sub-crustal viscosity are low, and similar to the depth averaged viscosity estimated for the asthenosphere beneath cratons (Dixon et al., 2004). Locally in the western USA, sub-lithopshere viscosities lower than 10^{20} Pa s have been explained by a high water content (Dixon et al., 2004; Li et al., 2008). It appears that the shallow mantle beneath Northern Baja has a low viscosity so that the mechanical lithosphere defined by a high viscosity is restricted to the crust. The high temperatures and small grain sizes can explain the low viscosity of the sub-crustal mantle in this area, with deformation occurring by a combination of dislocation creep and diffusion creep. A thin, chemically depleted, relatively dry, conductively cooled boundary layer occurs in the shallow mantle, which is mechanically weak

because of the high temperatures and small grain sizes. The Northern Baja lithosphere is thus an interesting case, where the thermal, chemical and mechanical nature of the lithosphere are significantly different.

8. Conclusion

Microstructural analysis of the San Quintin xenolith suite suggests that the lithosphere beneath the Baja California peninsula has been subject to deformation processes involving recrystallisation and melt–rock interaction. The xenoliths provide evidence for a very intense deformation within a possibly active shear zone in the shallow upper mantle (Cabanes and Mercier, 1988) giving fine-grained microstructures (Luhr and Aranda-Gómez, 1997). The deeper less deformed xenoliths have stronger CPO and seismic anisotropy compared to the finer grained more strongly deformed shallow xenoliths. It is inferred that recrystallisation, grain boundary sliding and melt–rock interaction all contributed to the weakening of the CPO in the fine grained xenoliths. The consequence is a decrease in seismic velocity for P- and S-waves. The difference in anisotropies would be associated with a seismic anomaly between the peridotites of up to 5.9% for P-waves and 4% for S-waves, while the P-wave decrease from lherzolites to pyroxenites reaches 7.6%. The CPOs indicate dominant [100] slip so that the fast seismic direction is sub-parallel to the flow direction. We suggest that surface wave anisotropy at shallow depths is produced by active flow in shear zones that accommodate the motion of Northen Baja relative to the Pacific plate. Estimates of the strain rate, stress and viscosity indicate that the shallow mantle beneath Northern Baja has a similar viscosity to the asthenosphere.

Appendix A. Supplementary information

Supplementary data associated with this article can be found in the online version at http://dx.doi.org/10.1016/j.epsl.2012.06.042.

References

Atwater, T., Stock, J., 1998. Pacific–North America plate tectonics of the Neogene Southwestern United States—an update. Int. Geol. Rev. 40, 375–402.

Basu, A.R., 1975a. Petrogenesis of Xenoliths from the San Quintin Volcanic Field, Baja California. Ph.D. Thesis. University of California, Davis, 229 pp.

Basu, A.R., 1975b. Hot spots, mantle plumes and a model for the origin of ultramafic xenoliths in alkali basalts. Earth Planet. Sci. Lett. 28, 261–274.

Basu, A.R., 1977. Textures, microstructures and deformation of ultramafic xenoliths from San Quintin, Baja California. Tectonophysics 43, 213–246.

Basu, A.R., Murthy, V.R., 1977. Ancient lithospheric lherzolite xenolith in alkali basalt from Baja California. Earth Planet. Sci. Lett. 35, 239–246.

Bell, D.R., Rossman, G.R., Maldener, J., Endisch, D., Rauch, F., 2003. Hydroxide in olivine: a quantitative determination of the absolute amount and calibration of the IR spectrum. J. Geophys. Res. 108 (B2), 2105, http://dx.doi.org/10.1029/2001JB000679.

Ben Ismaïl, W., Mainprice, D., 1998. An olivine fabric database: an overview of upper mantle fabrics and seismic anisotropy. Tectonophysics 296, 145–157.

Cabanes, N., Mercier, J.-C.C., 1988. Insight into the upper mantle beneath an active extensional zone: the spinel-peridotite xenoliths from San Quintin (Baja California, Mexico). Contrib. Mineral. Petrol. 100, 374–382.

Carter, N.L., Avé Lallement, H.G., 1970. High temperature flow of dunite and peridotite. Geol. Soc. Am. Bull. 81, 2181–2202.

De Kloe, R., 2001. Deformation mechanisms and melt nano-structures in Experimentally deformed olivine–orthopyroxene rocks with low melt fractions. An electron microscopy study. Ph.D. Thesis. Utrecht University, 173 pp.

Dixon, J.E., Dixon, T.H., Bell, D.R., Malservisi, R., 2004. Lateral variations in upper mantle viscosity. Earth Planet. Sci. Lett. 222, 451–467.

Hirth, G., Kohlstedt, D.L., 2003. Rheology of the upper mantle and the mantle wedge: a view from the experimentalists. In: Eiler, J. (Ed.), Inside the subduction factory. Geophys. Monographs, 138; 2003, pp. 83–105.

Holtzman, B.K., Kendall, J.-M., 2010. Organized melt, seismic anisotropy, and plate boundary lubrication. Geochem. Geophys. Geosyst. 11, Q0AB06, http://dx.doi.org/10.1029/2010GC003296.

Jung, H., Karato, S., 2001. Water-induced fabric transitions in olivine. Science 293, 1460–1463.

Karato, S., 1995. Effects of water on seismic wave velocities in the upper mantle. Proc. Jpn. Acad. 71, 61–66.

Karato, S.-I., Jung, H., Katayama, I., Philip Skemer, P., 2008. Geodynamic significance of seismic anisotropy of the upper mantle: new insights from laboratory studies. Annu. Rev. Earth Planet. Sci. 36, 59–95.

Katayama, I., Jung, H., Karato, S.-I., 2004. New type of olivine fabric at modest water content and low stress. Geology 32, 1045–1048.

Kneller, E.A., van Keken, P.E., Karato, S.-I, Park, J., 2005. B-type olivine fabric in the mantle wedge: insights from high-resolution non-Newtonian subduction zone models. Earth Planet. Sci. Lett. 237, 781–797.

Lenoir, X., Garrido, C.J., Bodinier, J.-L., Dautria, J.-M., Gervilla, F., 2001. The recrystallisation front of the Ronda peridotite: evidence for melting and thermal erosion of subcontinental lithospheric mantle beneath the Alboran basin. J. Petrol. 42, 141–158.

Lewis, J.L., Day, S.M., Magistrale, H., Castro, R.R., Astiz, L., Rebollar, C., Eakins, J., Vernon, F.L., Brune, J.N., 2001. Crustal thickness of the peninsular ranges and gulf extensional province in the Californias. J. Geophys. Res. 106 (B7), 13599–13611.

Li, Z.-X.A., Lee, C.-T.A., Peslier, A.H., Lenardic, A., Mackwell, S.J., 2008. Water contents in mantle xenoliths from the Colardo Plateau and vicinity: implications for the mantle rheology and hydration-induced thinning of continental lithopshere. J. Geophys. Res. 113, B09210, http://dx.doi.org/10.1029/2007/JB005540.

Lloyd, G.E., Schmidt, N.H., Mainprice, D., Prior, D.J., 1991. Crystallographic textures. Mineral. Mag. 55, 331–345.

Long, M.D., 2010. Frequency-dependent shear wave splitting and heterogeneous anisotropic structure beneath the Gulf of California region. Phys. Earth Planet. Inter. 182, 59–72.

Luhr, J.F., Aranda-Gómez, J.J., 1997. Mexican peridotite xenoliths and tectonic terranes: correlations among vent location, texture, temperature, pressure, and oxygen fugacity. J. Petrol. 38, 1075–1112.

Luhr, J.F., Aranda-Gómez, J.J., Housh, T.B., 1995. San Quintin volcanic field, Baja California Norte, México: geology, petrology, and geochemistry. J. Geophys. Res. 100, 10353–10380.

Mainprice, D., 1990. An efficient fortran program to calculate seismic anisotropy from the lattice preferred orientation of minerals. Comput. Geosci. 16, 385–393.

Mehl, L., Hacker, B.R., Hirth, G., Kelemen, P.B., 2003. Arc-parallel flow within the mantle wedge: evidence from the accreted Talkeetna arc, south central Alaska. J. Geophys. Res. 108 (B8), 2375, http://dx.doi.org/10.1029/2002JB002233.

Mercier, J.-C.C., Nicolas, A., 1975. Textures and fabrics of upper mantle peridotites as illustrated by xenoliths from basalts. J. Petrol. 16, 454–487.

Nagy, E.A., Stock, J.M., 2000. Structural controls on the continent–ocean transition in the northern Gulf of California. J. Geophys. Res. 105, 16251–16269.

Nicolas, A., 1986. Structure and petrology of peridotites: clues to their geodynamic environment. Rev. Geophys. 24, 875–895.

Nicolas, A., Poirier, J.P., 1976. Crystalline Plasticity and Solid State Flow in Metamorphic Rocks. Wiley, London.

Obrebski, M., Castro, R.R., Valenzuela, R.W., van Benthem, S., Rebollar, C.J., 2006. Shear-wave splitting observations at the regions of northern Baja California and southern Basin and Range in Mexico. Geophys. Res. Lett. 33, L05302, http://dx.doi.org/10.1029/2005GL024720.

Palasse, L.N., 2003. La lithosphère subcontinental au-dessus d'un panache mantellique: Etude pétrophysique des nodules de péridotite du Massif Central (France). M.Sc. Thesis. Université Montpellier II, 60 pp.

Paterson, M.S., 1982. The determination of hydroxyl by infrared absorption in quartz, silicate glasses and similar materials. Bull. Minéral. 105, 20–29.

Persaud, P., Pérez-Campos, X., Clayton, R.W., 2007. Crustal thickness variations in the margins of the Gulf of California from receiver functions. Geophys. J. Int. 170, 687–6690, http://dx.doi.org/10.1111/j.1365–246X.2007.03412.x.

Peslier, A.H., Luhr, J.F., 2006. Hydrogen loss from olivines in mantle xenoliths from Simcoe (USA) and Mexico: mafic alkalic magma ascent rates and water budget of the sub-continental lithosphere. Earth Planet. Sci. Lett. 242, 302–319.

Peslier, A.H., Luhr, J.F., Post, J., 2002. Low water contents in pyroxenes from spinel-peridotites of the oxidized, sub-arc manttle wedge. Earth Planet. Sci. Lett. 201, 69–86.

Plattner, C., Malservisi, R., Govers, R., 2009. On the plate boundary forces that drive and resist Baja California motion. Geology 37, 359–362.

Plattner, C., Malservisi, R., Dixon, T., Sella, G., Lafemina, P., Fletcher, J., Suarez-Vidal, F., 2007. New constraints on relative motion between the Pacific plate and Baja California microplate (Mexico) from GPS measurements. Geophys. J. Int. 170, 1373–1380, http://dx.doi.org/10.1111/j.1365–246X.2007.03494.x.

Soustelle, V., Tommasi, A., Demouchy, S., Ionov, D.A., 2010. Deformation and fluid-rock interaction in the supra-subduction mantle: microstructures and water Contents in peridotite xenoliths from the Avacha Volcano, Kamchatka. J. Petrol. 51, 363–394.

Stock, J.M., Hodges, K.V., 1989. Pre-Pliocene extension around the Gulf of California and the transfer of Baja California to the Pacific Plate. Tectonics 8, 99–115.

Storey, M., Rogers, G., Saunders, A.D., Terell, D.J., 1989. San Quintin volcanic field, Baja California, Mexico: 'within-plate' magmatism following ridge subduction. Terra Nova 1, 195–202.

Tommasi, A., Godard, M., Coromina, G., Dautria, J.-M., Barsczus, H., 2004. Seismic anisotropy and compositionally induced velocity anomalies in the lithosphere above mantle plumes: a petrological and microstructural study of mantle xenoliths from French Polynesia. Earth Planet. Sci. Lett. 227, 539–556.

Trampert, J., van Wettum, A., Clayton, R., Castro, R., Rebollar, C., Perez-Vertti, A., 2003. New array monitors seismic activity near the Gulf of California, Mexico. EOS 84 (4), 29–32.

Van der Wal, D., Chopra, P.N., Drury, M., Fitz Gerald, J.D., 1993. Recrystallised grain-size stress relationships in experimentally deformed olivine-rocks. Geophys. Res. Lett. 20, 1479–1482.

Vauchez, A., Tommasi, A., 2003. Wrench faults down to the asthenosphere: geological and geophysical evidence and thermo-mechanical effects. In: Storti, F., Holdsworth, R.E., Salvini, F. (Eds.), Intraplate Strike-Slip Deformation Belts, vol. 210. Geological Society of London, Special Publication, pp. 15–34.

Wang, Y., Forsyth, D.W., Savage, B., 2009. Convective upwelling in the mantle beneath the Gulf of California. Nature 462, 449–502.

Zeuch, D.H., Green, H.W., 1977. Naturally decorated dislocations in olivine from peridotite xenoliths. Contrib. Mineral. Petrol. 62, 141–151.

Zhang, X., Paulssen, H., Lebedev, S., Meier, T., 2007. Surface wave tomography of the Gulf of California. Geophys. Res. Lett. 34, L15305, http://dx.doi.org/10.1029/2007GL030631.

Zhang, X., Paulssen, H., Lebedev, S., Meier, T., 2009. 3D shear velocity structure beneath the Gulf of California from Rayleigh wave dispersion. Earth Planet. Sci. Lett. 279, 255–262.